Vibrational Raman studies of amorphous solid interfaces

Peter D. Persans
Department of Physics and Center for Integrated Electronics, Rensselaer Polytechnic Institute, Troy, New York 12180-3590
(Received 10 June 1988; revised manuscript received 15 September 1988)

We report and quantitatively analyze vibrational Raman spectra of (hydrogenated amorphous silicon)–(silicon nitride) and silicon-germanium interfaces. Periodic multilayer structures were deposited by plasma-assisted chemical-vapor deposition with layer repeat distances from 1.5 to 20 nm. The repeat distance was varied in order to vary the fraction of the multilayer structure which is near the interface between the two materials and thereby separate interface vibrational structure from bulk properties. We find significant distortions in amorphous silicon material near the silicon–(silicon nitride) interface with estimated deformation energy of almost 1 eV per silicon atom. This distortion could be due either to interface strain from network mismatch or to incorporation of excess nitrogen in the *a*-Si near the interface. The distortion is confined to within two monolayers of each interface. No excess deformation is found near the silicon-germanium interface. We also report the observation of size effects on the optical properties of *a*-Si:H using resonant Raman scattering.

I. INTRODUCTION

Lattice mismatch in epitaxial crystalline materials can determine the electronic quality of epitaxial heterojunctions[1] and may even affect the macroscopic mechanical properties of superlattice structures.[2] We expect this also to be the case for amorphous heterojunctions and multilayers. A significant fraction of the current research on growth of epitaxial semiconductors is on the detailed manner in which strain is accommodated (i.e., misfit dislocations in GaAs/Si) and the spatial extent and electronic ramifications of the presence of these defects. Our understanding of the covalent amorphous-solid–amorphous-solid heterojunction interface is at a much more primitive stage. This is in part due to the fact that the interface structure is much more difficult to model when we only know local bonding arrangements and statistical structure of the heterojunction materials, as opposed to the crystalline long-range structure. Our understanding of crystalline heterojunction structure is also aided by the availability of specific experimental techniques such as ion channeling[3] and transmission electron microscope imaging,[4] which take advantage of the regular crystalline structure to enhance contrast of defects. Studies of amorphous heterojunctions are of necessity less direct.

An understanding of the relationship between interfacial network mismatch and network distortion, strain, and resultant electronic properties of amorphous heterojunctions may prove to be very important for the engineering of new amorphous materials and devices. A few of the important questions are the following. How does network mismatch manifest itself in amorphous materials? How is network mismatch relieved at amorphous heterojunctions? Are electronic defects such as dangling bonds intrinsic to mismatched interfaces? What structural criteria are important in deciding whether an interface can have a low defect density?[5] We note that these questions have not been satisfactorily answered for any but the most simple crystalline heterojunctions.

In this paper we report and quantitatively analyze the vibrational Raman spectra of (hydrogenated amorphous silicon)–(amorphous silicon nitride) (*a*-Si:H/*a*-SiN_x:H) and (amorphous silicon–amorphous germanium) (*a*-Si:H/*a*-Ge:H) interfaces in order to elucidate the magnitude and spatial extent of network distortions near interfaces. These two systems serve as structurally extreme cases of the amorphous heterojunction. Amorphous silicon and germanium are structurally similar;[6] they are both locally tetrahedral, their bond lengths differ by about 5%, and bond-angle fluctuations are similar. On the other hand *a*-Si and *a*-SiN_x differ radically in network structure; the average Si—N bond length is 40% shorter than the Si—Si bond. We therefore anticipate substantial network rearrangement in one or both materials in order to fit these two networks together.

In Sec. II we discuss experimental details, including sample preparation, general sample characterization, sample selection strategy, and quantitative aspects of the Raman measurements. In Sec. III A we discuss the results and analysis of Raman scattering on a series of silicon–nitride periodic multilayers, and in Sec. III B we discuss measurements on silicon–germanium multilayers. In Sec. IV we draw some general conclusions with regard to amorphous heterojunctions and suggest areas for new work.

II. EXPERIMENTAL DETAILS

A. Sample preparation

Samples with a total thickness of approximately 1 μm were prepared by low-pressure plasma-assisted chemical-vapor deposition (PACVD) in a 13.56-MHz capacitive reactor described in detail elsewhere.[7] Multilayers were deposited by alternating feed gases. Pure SiH_4 was used for the *a*-Si:H layers, 10% GeH_4 in H_2 for the *a*-Ge:H layers, and mixtures of 5:1 NH_3 to SiH_4 for SiN_x:H. In-

dividual sublayers were between 1 and 10 nm in thickness; thus a typical film might have between 10 and 500 layer repeats. For *a*-Si:H/*a*-Ge:H films the gas flow was switched and rf power was continuous. For *a*-Si:H/*a*-SiN_x:H films the plasma was interrupted for 10 s during gas exchange for some samples, in order to check that contamination from layer to layer was minimal. No differences were found between continuous and interrupted depositions. The base vacuum of the deposition system was 10^{-8} Torr. Typical film growth conditions were gas flow rate, 85 sccm; pressure, 30 mTorr; rf power, 5 W; substrate temperature, 240 °C. Film growth rate was about 1 Å/s, whereas the gas exchange time was about 1 s. Films were grown on the anode (grounded) electrode of the reactor. Substrates were "suprasil" quartz or crystalline Si.

All depositions were computer controlled and monitored. System pressure, flow rates, temperatures, and switching times were automatically controlled. Optical emission from the plasma and induced dc bias voltage were monitored in order to ensure ignition of the plasma and stability of growth conditions. Polarized optical reflectivity of growing films was monitored and analyzed[8,9] in order to ensure sample uniformity. Samples which did not meet ignition and growth criteria requiring less than 2% drift in growth rates were rejected. The relative thicknesses of the sublayers could be determined by *in situ* optical as well as by *ex situ* x-ray[10] and average index measurements on films.

In order to bring out differences in samples due to interfaces, the overall composition of each series of films was kept constant by keeping the ratio of growth times for sublayers in a repeat fixed while changing the repeat time. The average Si, Ge, and N composition of the multilayer films was measured by Rutherford backscattering (RBS) and the H content was measured by ^{15}N nuclear resonant reaction by Lanford and co-workers at The State University of New York at Albany.[11] The sublayer thicknesses were found by combining growth rate, composition, and optical data. The N-to-Si ratio in bulk *a*-SiN_x:H was 0.97, consistent with fits to the average composition of layered samples. For the *a*-Si:H/*a*-SiN_x:H series $d_S = 0.85 d_N$ (d_S is the silicon sublayer thickness and d_N is the nitride sublayer thickness) while the repeat distance $d_r = d_S + d_N$ was varied from 1.5 to 17 nm. For *a*-Si:H/*a*-Ge:H periodic multilayers the average composition was held constant with almost equal atomic fraction of the two principle elements while the repeat distance was varied from 1.0 to 20 nm.

B. Raman scattering and optics

Raman measurements were carried out at room temperature in near-backscattering configuration. Scattered light with polarization perpendicular to the excitation polarization (*VH*) was collected. Excitation using either the 514.5- or 488.0-nm Ar^+ laser line or the 568.2-nm Kr^+ line was focused at normal incidence onto the surface of the (specular) sample in a 0.2×2 mm^2 spot through a 5-mm hole in a 50-mm-diam spherical collection mirror. Specularly reflected light was reflected back out of the sample chamber through the same hole. Scattered light was focused onto the entrance slit of the monochromator, the image being magnified by about a factor of 5 in the process. The weak Raman signal was analyzed with either a triple monochromator [consisting of a premonochromator with two 0.25-m stages operated in subtractive dispersion and a 0.7-m spectrograph (Spex 1877B Triplemate)] for low resolution or a double monochromator [consisting of two 1-m monochromators in additive dispersion (Jobin-Yvon HG2000M)] for high resolution studies. The triple monochromator was coupled to a cooled optical multichannel analyzer (PAR OMA III with 1420 detector) and the double monochromator to a cooled RCA 31034A photomultiplier. Both detectors were operated in photon counting mode at −30 °C. Clean He gas was continuously blown onto the sample surface in order to eliminate Raman scattering from N_2 in the air. The laser power absorbed in the sample was kept below 1 W/cm^2 in order to avoid sample heating. The absence of significant heating was confirmed by measuring the Raman spectrum of one sample as a function of power. We estimate that the sample temperature was always below 50 °C. Laser plasma lines were eliminated from the spectra by the use of a pair of Pellin-Broca prisms and a pinhole through which the desired laser line was focused.

In order to quantitatively analyze the Raman data it is necessary to correct the spectral intensities for sample volume and collection optics differences. When the sample is thick relative to the optical absorption depth, the excitation volume (and hence the Raman intensity) depends inversely upon the optical absorption coefficient of the sample at the laser and Raman shifted wavelengths. Thus it is important to accurately measure the optical absorption coefficient in order to properly normalize the Raman data. Furthermore, the fraction of the light which escapes from the sample surface and falls within the collection cone of the optics depends upon the index of refraction of the sample. Optical transmission measurements were carried out at room temperature on samples on SiO_2 substrates using a Varian 2390 spectrophotometer. Both optical absorption and index measurements can be extracted from these measurements in a straightforward way. In Fig. 1(a) we show the optical absorption coefficient plotted as a function of photon energy for the *a*-Si:H/*a*-SiN_x:H series. In Fig. 1(b) we have plotted the data from Fig. 1(a) as $(\alpha h\nu)^{1/2}$ in order to determine the optical gap, E_G. A summary of structural and optical data is given in Table I. Optical absorption data for the *a*-Si:H/*a*-Ge:H series have been previously published.[12,13]

We take advantage of the following properties of the samples in order to simplify the quantitative analysis of the Raman spectra: (i) The optical absorptance of individual sublayers is small, $\alpha d_r \ll 1$; (ii) the repeat distance d_r (< 10 nm) is much less than the optical wavelength in the sample (150 nm); and (iii) the total thickness d_T should be such that $\alpha d_T > 1$ in order to minimize substrate interference effects. Under these conditions the Raman scattered intensity I_R is given by

$$I_R = Cf(\theta)F_0(1-R)^2[1-\exp(-2\alpha d_T)] \times \left[\sum_i K_i d_i n_i\right] \Big/ (2\alpha n d_r) ,$$

where the sum is over sublayers in a single repeat, K_i is the Raman cross section for the material in the ith layer, F_0 is the incident flux, C is the product of detector efficiency (about 0.1) and monochromator throughput (about 0.1), R is the reflectivity of the sample front surface, α and n are the optical average absorption coefficient and refractive index of the layered effective medium, and n_i is the refractive index of the ith layer. The factor $f(\theta)=[1-\cos(\theta)]/2$ takes into account the solid angle within the sample from which scattered light can escape into the collection optics. The internal collection angle θ is determined by sample index and collection optics. The external collection angle θ_e is simply $\tan^{-1}(L/D)$ where D is the sample–collection-lens distance and L is the collection-lens radius. The internal collection angle is related to the external collection angle by Snell's law, $\sin\theta_c = n\sin\theta$.

For a given wavelength and sample series C and F_0 were kept constant. The factors $f(\theta)$, $(1-R)^2$, and $d_{\text{eff}}=[1-\exp(-\alpha d_T)]/2\alpha$ can be calculated using known optical properties of the samples. For $\theta_e = 30°$ and $n=3$, then $\theta = 9.6°$ and $(1-R)^2 f(\theta) = 0.0038$. Thus it is possible to deduce the change in the Raman cross section K_i by making straightforward optical corrections. Index corrections from sample to sample are relatively small because the composition for each series was held constant. In practice it is difficult to measure intensity absolutely and thus measure K_i. In this paper we measure relative intensities. Measurements are referenced to bulk a-Si:H and to one another for internal consistency.

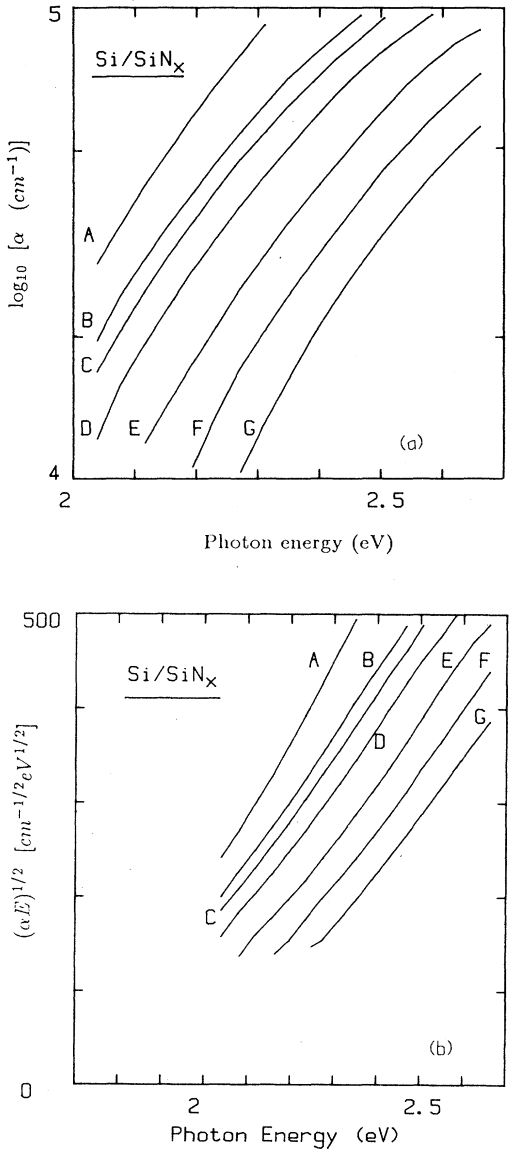

FIG. 1. (a) Optical absorption coefficient α plotted against photon energy for a series of Si/SiN$_x$ multilayer films in which the layer repeat distance was varied from 1.5 to 17 nm. (b) $(\alpha h\nu)^{1/2}$ plotted against photon energy ($h\nu$) for the same samples as in (a).

III. RESULTS AND DISCUSSION

A. Silicon–(silicon nitride)

1. Raman results: Si/SiN$_x$

In Fig. 2 we show Stokes scattered Raman spectra taken with 568.2-nm excitation for three representative silicon–(silicon nitride) superlattice films with silicon sublayer thickness d_S of 0.7 to 7.8 nm. For thick Si sublayers ($d_S > 5$ nm) the spectrum in the range 50 to 650 cm^{-1} is the same as that of pure a-Si:H aside from a featureless background. The scattered light spectrum of a-SiN$_x$:H as grown for this experiment is featureless from 80 to 1000 cm^{-1}. (It is probable that fluorescence contributes to this intensity.) The major vibrational features measured in the multilayer spectrum at 150, 320–400, and 475 cm^{-1} correspond to transverse acoustic (TA), longitudinal acoustic and optic (LA and LO), and transverse optic (TO) -like modes in a-Si:H, respectively.[14,15] The sharp feature at 520 cm^{-1} is due to the crystalline Si substrate. The spectra have been normalized to the same TO mode height for display purposes. Since it is clear that the spectra are not simply the superposition of the spectrum of bulk a-Si:H and a-SiN$_x$:H, it is necessary to describe the spectra with a number of parameters. The major parameters which describe the spectra are the TO mode height (H_O) and position, the TA mode height (H_A) and position, the background intensity (B) scaled using Eq. (1), and the width of the TO mode. [We use the half width at half maximum (HWHM) Δ measured on the high-energy side of the peak in order to avoid interference from the LA and LO modes.]

The TO peak width is more easily measured using strongly absorbed excitation which does not penetrate through the sample to the substrate, thus eliminating the sharp peak at 520 cm^{-1}. In Fig. 3 we show Raman spectra in the region of the TO peak excited with 488.0-nm radiation.

TABLE I. Structural and optical data for a-Si:H/a-SiN$_x$:H multilayers

	Repeat distance (nm)	Silicon thickness (nm)	Index n (at 2.54 eV)	Index n (at 2.2 eV)	Absorption coefficient (cm^{-1}) (at 2.54 eV)	Absorption coefficient (cm^{-1}) (at 2.2 eV)	Optical gap (eV)
A	Bulk Si		4.7	4.5	1.8×10^5	5.4×10^4	1.70
B	17.0	7.8	3.52	3.38	1.1×10^5	3.75×10^4	1.70
C	8.5	3.9	3.50	3.35	1×10^5	3.25×10^4	1.74
D	5.5	2.5	3.48	3.33	8.5×10^4	2.5×10^4	1.79
E	3.3	1.5	3.44	3.28	6.5×10^4	1.6×10^4	1.89
F	2.25	1.0	3.39	3.23	5×10^4	1×10^4	1.97
G	1.6	0.7	3.25	3.14	3.7×10^4	7×10^3	2.05

We summarize the results from Figs. 2 and 3 in Table II. We have scaled the data by the factor $S=F_0[1-\exp(-2\alpha d_T)](1-R)^2 f(\theta)/2\alpha$. The quantity $(H_O-B)/S$ is thus the height of the TO mode minus the background divided by the effective volume of the sample probed, the geometric collection efficiency, and the incident laser power. We shall call this normalization procedure S normalization throughout this paper. All peak heights as well as the background have been referenced to the height of the S-normalized TO mode in bulk a-Si:H for a given excitation line.

Certain features of the data are clear from inspection of Figs. 2 and 3 and Table II. First, the ratio of the TA peak height $[(H_A-B)/S]$ to the TO peak height $[(H_O-B)/S]$ increases as d_S decreases. This is mostly due to a relative decrease in the height of the TO mode. If we integrate the total counts under the TO peak by taking twice the area under the high-energy side of the TO peak (I_O/S) and compare that to the TA-mode intensity, we find that ratio is nearly constant. This observation is coupled to the fact that the width of the TO mode Δ increases as d_S decreases.

The S-normalized integrated intensity under both the TA and TO modes as well as the total intensity, after subtracting the flat background, are independent of d_S for 488-nm excitation. On the other hand, the S-normalized integrated intensity under the TA and TO peaks as well as the total normalized intensity *are* dependent upon d_S for 568.2-nm excitation. The intensity drops by about a factor of two as d_S is decreased from 2.5 to 0.7 nm. The intensity of the background increases as d_S decreases for 488-nm excitation, whereas it remains nearly constant for 568.2-nm excitation.

The changes in the Raman spectrum of a-Si/a-SiN$_x$ can be broken down into a small number of basic observations. (i) The intensity of scattering from the a-Si lay-

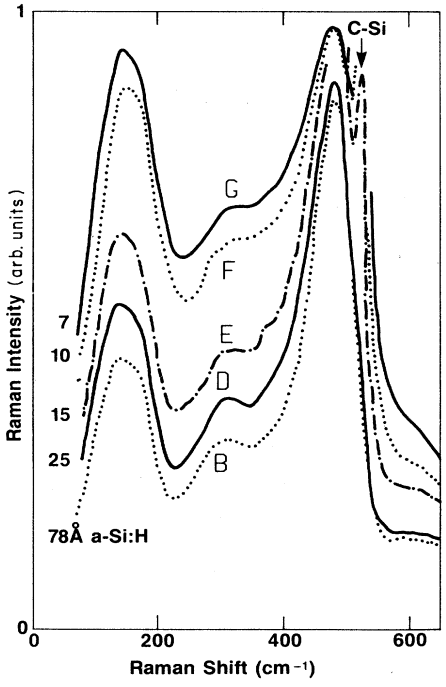

FIG. 2. Raman spectra for several a-Si:H/a-SiN$_x$:H multilayer samples. Laser excitation was 568.2 nm and the sample substrate was crystalline Si. The peak at 520 cm^{-1} is due to the crystalline Si substrate.

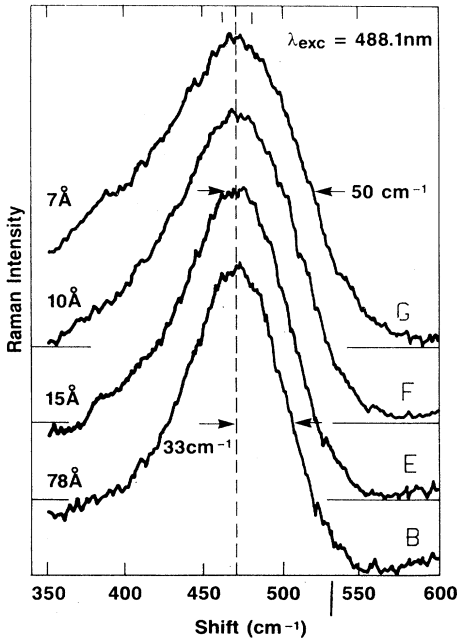

FIG. 3. Raman spectra in the region of the TO mode for several a-Si:H/a-SiN$_x$:H multilayer samples. Excitation was with the Ar^+ 488-nm laser line.

TABLE II. Raman spectrum parameters for 488- and 568.2-nm excitation. B, background level at 650 cm^{-1}; S, volume and index normalization factor equal to $F_0 d_{eff}(1-R)^2 f(\theta) n/ns$; H_O, height of TO mode at peak; H_A, height of TA mode at peak; I_O, integrated intensity under TO mode (background subtracted).

	HWHM (cm^{-1})	B/S	$(H_O-B)/S$	$(H_A-B)/S$	I_0/S	B/S	$(H_O-B)/S$	$(H_A-B)/S$	I_0/S
Wavelength	488	488	488	488	488	568	568	568	568
A	33	0.08	1.00	0.26	1.00	0.05	1.00	0.45	1.00
B	33	0.23	1.10	0.33	1.03	0.18	1.16	0.48	1.07
C	33	0.24	0.92	0.31	0.87	0.16	1.02	0.41	0.97
D	37	0.28	0.95	0.33	1.00	0.16	0.97	0.50	1.08
E	39	0.31	0.81	0.36	0.90	0.18	0.71	0.40	0.81
F	42	0.35	0.59	0.34	0.73	0.14	0.40	0.34	0.48
G	50	0.33	0.50	0.28	0.75	0.14	0.26	0.25	0.36

ers is dependent on the silicon sublayer thickness and excitation energy. (ii) The width of the silicon TO mode increases as d_S is decreased below 5 nm. (iii) The positions of the TO and and TA modes are independent of layer thickness. (iv) An excitation-energy dependent change is observed in the intensity of the flat background B. We shall discuss each of these effects separately below.

(i) We believe that the change in normalized intensity of scattering from the *a*-Si:H layers can be naturally explained by the resonance Raman effect and a size-shift in the optical properties of *a*-Si:H in layers. Resonance Raman scattering studies have been performed on *a*-Si (Ref. 14) and *a*-Si:H (Ref. 15) with similar conclusions for both materials. A peak is observed in the resonance-enhanced cross section at about 3.2 eV with a sharp decrease in intensity by a factor of 4 as excitation energy is lowered to 2.6 eV. There is a plateau in the cross section from about 2 to 2.5 eV and a very rapid roll-off in intensity when the excitation energy is decreased below 2 eV. The position of the edge of the 2-eV roll-off depends on the bandgap of the *a*-Si:H material (which is determined by preparation conditions[16]) and shifts up as the band gap shifts up.

In Refs. 14 and 15 the resonance spectra were measured by varying the excitation energy. In the present work the *band gap* was varied by varying d_S. We plot in Fig. 4 the integrated intensity of the TO mode in the present experiment as a function of the difference between the excitation energy and the band gap of the layered material. The normalized intensity with 488 nm (2.54 eV) excitation is insensitive to the band gap of the multilayer because this energy is on a relatively flat section of the resonance spectrum. The intensity of the TO mode drops slightly with decreasing d_S for 514.5 nm (2.41 eV) excitation. On the other hand the normalized intensity with 568.2 nm (2.18 eV) excitation drops off rapidly for $d_S < 1.5$ nm.

These observations support the argument that the bandgap energy of *a*-Si:H in ultrathin confined layers increases with respect to bulk material. Recently, analysis of ellipsometric and optical absorption data based on the assumption of a rough interface between *a*-Si:H and *a*-SiN_x (Refs. 17 and 18) was used to suggest that the apparent shift in E_G with decreasing d_S was largely due to optical effective medium rather than size effects. The present resonant Raman results involve the same assumptions for all three excitation energies. The different behavior for low-energy excitation versus high-energy excitation suggests that the optical properties of the *a*-Si:H layers must really change with d_S. The agreement between resonant Raman results from the literature and the present results indicate that band-gap shifts derived from extrapolation of optical absorption data actually do yield reliable measurements of size shifts. The physical origin of these shifts remains a controversial issue. Two possibilities are (a) quantum size shifts due to confinement of states near the band edges,[19,20] and (b) excess hydrogen or nitrogen near the interfaces.[11] Recent modulation spectroscopy studies strongly support the existence of a quantum size effect.[20]

(ii) The HWHM of the TO-like mode clearly increases as d_S is decreased. We shall focus on two aspects of this observation. First, we shall discuss the two limiting cases of thick ($d_S > 5$ nm) and thin ($d_S = 0.7$ nm) Si layers. Second, we shall discuss the quantitative changes in spectral shape with silicon sublayer thickness.

The TO-like mode width Δ in thick layers is the same as that of bulk *a*-Si:H prepared under similar conditions. It has been suggested by several groups[21–26] that the width of this mode correlates with rms deviations in the bond angle $\delta\theta = 6°-12°$ from the ideal tetrahedral bond angle of 109.4° in *a*-Si, *a*-Si:H, *a*-Ge, and *a*-Ge:H. The width $\Delta = 33$ cm^{-1} in the present thick Si multilayers is quite narrow and suggests that the bond-angle distribution is also narrow (i.e., that the present thick Si layers have comparable disorder to high-electronic-quality bulk films.)

The TO mode width $\Delta = 50$ cm^{-1} for the thinnest silicon sublayer ($d_S = 0.7$ nm) materials is nearly 1.7 times wider than Δ for bulk material. This result is in substantial agreement with measurements on similar *a*-Si:H/*a*-SiN_x multilayer samples by other groups.[27,28] One possible origin for the increase in width is increased structural disorder near the interfaces. When d_S is only 0.7 nm we should think of the structure as being mostly interface. We expect on simple bond-counting arguments[29] that approximately one-half of the Si atoms in the *a*-Si:H layer will be bonded to atoms in the nitride layers. Since the two networks must have very different local structures we expect that atoms bonded at or near the interface will have distorted bonding arrangements. This will show up

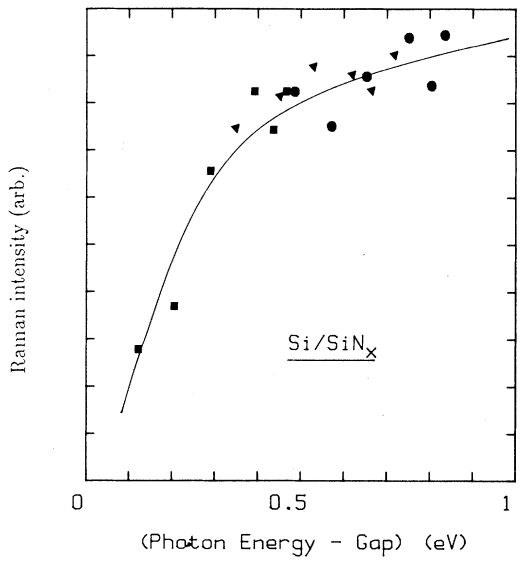

FIG. 4. Volume-normalized intensity of the TO-like mode in a-Si:H/a-SiN$_x$:H multilayers plotted as a function of the difference between the excitation energy and the optical bandgap of the layered material. Excitation energies were ●, 2.54 eV; ▲, 2.41 eV; ■, 2.18 eV. The solid line is a guide to the eye.

in the width of the Si TO-like mode.

We can estimate the energy stored in local bond-angle distortions in the Si near the interface by comparing the TO mode width in these experiments to measurements and theory for bulk a-Si. Recent theoretical calculations[22,30,31] on cluster models yield a correlation between bond-angle deviations and Raman TO mode width in a-Si. Beeman *et al.*[22] found a simple relationship: $\Delta=7.5+3\,\delta\theta$, where $\delta\theta$ is the rms bond-angle deviation. From this relationship we calculate that the rms bond-angle deviations in the $d_S=0.7$ nm and the $d_S=7.8$ nm samples are about 12° and 8°, respectively. The force constant k for bond bending in Si is[32] 9.2×10^3 dyn/cm. The average distortion energy U per bond can easily be found using $U=3k(r_B\,\delta\theta)^2$ where $r_B=2.4\times10^{-8}$ cm is the bond length. Taking $\delta\theta=12°$, we find $U=0.45$ eV/bond; for $\delta\theta=8.0°$, $U=0.2$ eV/bond. This is a very substantial fraction of the bond energy for band-edge states and we would expect this distortion energy to be observable by electronic or optical techniques. In fact a substantial broadening of the optical absorption edge has been reported in these and similar multilayers.[19,33]

There is a second, related interpretation for the increase in TO-like mode width with decreasing d_S. Incorporation of nitrogen into a-Si:H can lead to a similar change in the Raman spectrum.[34] This broadening of the TO mode in alloys has been interpreted as local Si—Si bond disorder induced by the incorporation of N. With this interpretation the estimate of bond-angle distortion energy in the previous paragraphs is still substantially valid, although we note that in alloys there may be other mechanisms for TO mode broadening. For example, the vibrational frequency of a Si—Si pair will be influenced by the force constants of the matrix in which it is embedded, which in turn depend on the local matrix composition. Proximity of N atoms could also lead to charge fluctuations from Si to Si which in turn alters bonding energies and vibrational frequencies. It is not possible in the present studies to separate structural disorder induced by N incorporation from chemical effects on the vibrational spectrum of Si—Si bonds or interface disorder as described above.

We can empirically estimate the amount of N incorporation in the Si layer necessary to explain the present results. We assume that the four monolayers of Si in each $d_S=0.7$ nm sublayer have composition a-SiN$_x$:H and we neglect interface effects. The spectrum would then be that of bulk a-SiN$_x$. Comparing the observed $\Delta=50$ cm^{-1} with the literature[34] we conclude that $x=0.3$ yields a consistent width. This amount of N is larger than estimated from RBS measurements on the same sample series[11] but is not out of the question. We have previously shown[12] that the interface between a-Si and a-Ge is indeed a fully mixed monolayer of alloy material therefore this possibility should not be excluded here. The most likely case is that the broadening is a combination of interface strain and alloying effects.

With the quantitative information which we have gained from these experiments we can calculate the distribution of interface-induced disorder as a function of distance from the interface. We have found that the entire a-Si:H Raman spectrum for layers intermediate between our two extreme samples ($d_S=0.7$ nm and bulk a-Si:H) can be modeled as the sum of the spectra from these two samples after the energy-independent background (B) has been subtracted from the spectra.

$$I(d_S,\omega)=\frac{[I(d_S=0.7\text{ mm},\,\omega)V_IK_I+I(\text{bulk},\omega)V_BK_B]}{(V_IK_I+V_BK_B)}\,,$$

where V_I and V_B are the volume fractions of interface ($d_S=0.7$ nm) and bulk components necessary to make the best fit to the spectra of intermediate d_S samples and K_I and K_B are the Raman cross sections for interface and bulk materials. We plot the results of this fit for both 488- and 568.2-nm excitation in Fig. 5. Data derived from 488-nm excitation is probably more reliable because resonant effects are larger for 568.2-nm excitation and we do not know how to rescale K_I when the interface is bordered by bulk a-Si:H as well as a-SiN$_x$:H. If the spectra were the simple sum of an interface of fixed thickness d_I and a bulklike region whose thickness d_B increases as d_S-d_I, then we would expect the V_I data to fall on a straight line in $1/d_S$ with intercepts at (0,0) and $(1/d_I,1)$. A straight line with intercept (9.5,1) yields a good fit to the data giving a value for d_I of about 1.1 nm. The implication of this result is that the network structure of a-Si:H is affected by the presence of the a-SiN$_x$ interface for only the first few monolayers into the Si and that outside of this region the network structure is that of bulk a-Si:H.

We calculated the distortion energy per bond for the thinnest layers earlier. Since we now know the spatial extent of the excess distortion we can estimate the surface tension in an as-grown a-Si:H/a-SiN$_x$:H interface. The

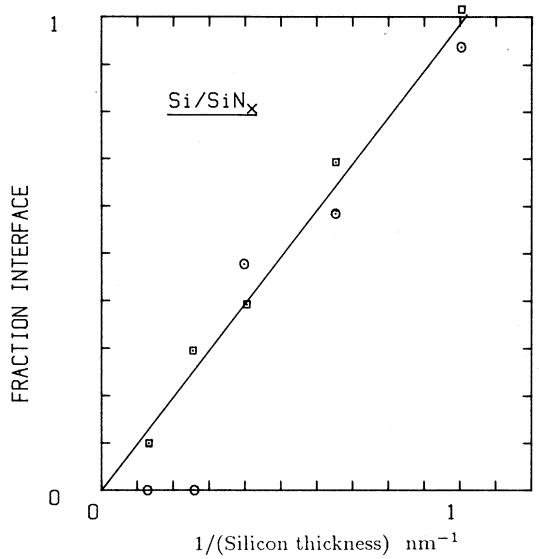

FIG. 5. Volume fraction of interfacelike a-Si:H ($d_s = 0.7$ nm) required to fit the spectra of other a-Si:H/a-SiN$_x$:H multilayer samples. Details of the fit are described in Sec. III A 1(ii).

atom density is about 5×10^{22} cm^{-3} yielding an average bond density of 10^{23} in a-Si. The distortion is found to extend over a 1.1-nm region for an interface pair. The total number of distorted bonds is thus 5×10^{15} cm^{-2}, with an average *excess* distortion energy of 0.25 eV/bond; thus the surface tension is of order 0.4 mJ cm^{-2}.

Similar conclusions with respect to the magnitude and extent of structural disorder near a-Si:H/a-SiN$_x$:H interfaces have been made by Lannin and co-workers.[27,28] In their analysis they assumed that the width of the TO mode was determined directly by the average disorder in the Si layer as opposed to the sum of the signals from sublayers with different disorder. This difference in analytical approach arises from a difference in assumptions about vibrational modes in a-Si. We have assumed that the important opticlike modes are quasilocal, in that the mode at one location in the network is independent of the network structure more than a few atom distances away; thus they can be treated by summing up signals from different regions of the sample. The validity of this assumption clearly depends on the scale of the inhomogeneity. In the Lannin work it is assumed that the vibrational structure is determined by a volume of a few hundred atoms, and therefore the network should be averaged before determining the effective Raman signal. In spite of this qualitative difference in analysis, they also concluded that a-Si:H approaches bulk properties outside a few monolayers of an interface. Since low-frequency modes due to zone-folded acoustic phonons have been observed,[35] it is clear that the quasilocal assumption breaks down in this regime; however, higher frequency optic modes may have a more local character. Our understanding of the spatial extent and coherence of vibrational modes in disordered systems is still quite incomplete.

The set of samples studied by Lannin and coworkers[27,28] (average composition varied substantially as d_S was varied) precluded the type of quantitative analysis carried out here. The width of the TO mode and the ratio of the TO height to TA height for their $d_S = 0.8$-nm sample is nearly the same as for the present $d_S = 0.7$-nm sample, indicating that the extent of interface disorder is not strongly dependent on sample preparation conditions.

(iii) The position of the TO-like mode can be used as a measure of average strain in crystalline layers. In crystalline Si the strain is easily observed as a shift due to average strain $\Delta V/V$ and also a broadening due to inhomogeneous strain. Typical shifts of a few cm^{-1} are observed for silicon on sapphire.[36] When a-Si is compressed the TO Raman mode shifts to higher energy[37] at the rate of 1 cm^{-1}k^{-1}bar and sharpens slightly. We therefore might expect to be able to observe similar shifts in the Raman spectrum of multilayers if there is a uniform strain in the thin layers. (Inhomogeneous strain cannot be distinguished from the broadening discussed in the previous section.) Fits to the data in Fig. 3 reveal that the TO-mode peak position is independent of layer thickness to within ±1 cm^{-1}. We conclude that the homogeneous strain $\Delta V/V$ is less than 0.002 in the amorphous silicon sublayer averaged over the laser spot size of 0.2 cm^2.

(iv) The intensity of the broad, featureless background which extends from <100 to >1000 cm^{-1} depends on laser excitation and repeat spacing. For the 2.18 eV (568.2 nm) laser line we find that the background is relatively small and independent of spacing. When the laser excitation energy is increased to 2.54 eV (488 nm), the relative intensity increases, especially for smaller repeat distances. It is not possible at this time to determine whether this background is Raman-scattered light or luminescence, although usually light emitted over such a wide energy range is due to luminescence. The wavelength and thickness dependence could be due to either resonant Raman effects or to excitation and emission energy dependence of luminescence in the SiN$_x$ layers.[38,39] An increase in luminescence intensity with increasing excitation energy is reasonable because absorption in SiN$_x$ increases with energy. Increasing excitation energy also increases the energy at which the scattered light is measured and thus may also increase luminescence from the nitride layers if the peak in intensity is above 2.5 eV. As the layer thickness is decreased, the overlap of wave functions in the silicon and nitride layers leads to an increase in the absorption (and emission) coefficients in the nitride layers which could account for increased luminescence from smaller spacings. Wave-function overlap effects have been observed by electroabsorption measurements in silicon–(silicon carbide) multilayers.[40]

2. *Related observations and discussion: Si/SiN$_x$*

The present results can be related to other measurements on similar multilayer materials. The average ratio of N to Si atoms, C_N, was determined for the same series of samples using Rutherford backscattering spectroscopy (RBS). We have previously[11,41] reported a small increase in C_N with decreasing d_r, which indicates either extra nitrogen in the silicon near the interfaces or slightly thicker nitride layers than the bulk growth rate suggests. The increase in N is consistent with an increase in each nitride layer thickness by 0.08 nm or about 20% N in the Si

monolayers closest to the nitride (about 0.4 nm per interface pair). As we noted earlier, this is about one-half of the excess N needed to explain the broadening of the Raman TO mode by alloy disorder alone.

The average hydrogen content C_H was measured by ^{15}N nuclear resonant reaction as a function of d_r.[11,41] It was found that C_H rises linearly with $1/d_r$ indicating 0.4×10^{15} cm^{-2} excess H per interface. Infrared absorption studies[11] indicate that most of the excess H is bonded within two monolayers of the interfaces to Si which is back-bonded to N. A smaller amount (about 1×10^{14} cm^{-2}) is bonded in dihydride form in a ten-monolayer thickness near the interfaces.

The density of electronically active defects near the interfaces is much lower than the H content. It is unlikely that 10^{12} defects/cm^2 would be important in the relaxation of strain, but it is certainly electronically significant. Electroabsorption measurements[7,33,42] reveal high internal fields which are due to charged defects near the interfaces. The fields observed require about 6×10^{12} charges/cm^2 per interface pair distributed over a width of 2 nm in the Si layer. Other measurements of defect density such as optical absorption,[7,33] luminescence,[43,44] and photoconductivity[45] yield much lower densities. For example, electron paramagnetic resonance[46] on similar multilayers yields a dangling bond density of only 1.3×10^{10} cm^{-2} per interface. EPR clearly measures only a small subset of the defects at the interface. It is not clear which if any of these electronic defects are related to intrinsic network mismatch. The presence of hydrogen and other low-level impurities is expected to have a large effect on the nature and number of electronic defects. It has been demonstrated that the electronically active interface defect density depends sensitively on preparation conditions for plasma-deposited materials,[47] whereas Raman scattering results seem to be insensitive to deposition conditions. A strong correlation between electron spin density and Raman TO mode width has been found for unhydrogenated bulk a-SiN$_x$,[34] however, when hydrogen is also incorporated during growth the correlation becomes much weaker and the spin density is nearly independent of x (2×10^{17} cm^{-3}) for $x>0.1$.[35] In the alloy materials H incorporation also leads to a reduction in TO mode width relative to unhydrogenated material of the same N-to-Si ratio. Since H can passivate electronic defects with high efficiency, the absence of good structure–defect-density correlation is not surprising at this stage. We note that the density of midgap states in plasma deposited a-Si:H can vary by more than an order of magnitude with only small changes in the deposition conditions.

B. Silicon–germanium

1. *Raman results and analysis: Si/Ge*

Raman scattering studies of the a-Si:H/a-Ge:H interface have focused on the extent of intermixing of the two principle components.[12,29,35,48,49] It has been demonstrated that as-deposited plasma materials have one to two monolayers of intermixed Si and Ge at each interface. In the present study however we will focus on the extent of disorder in the sublayer materials induced by the presence of the interface. In Fig. 6(a) we show the Raman spectrum of an a-Si:H/a-Ge:H, multilayer with $d_r=2.4$ nm. We have previously shown that this spectrum can be modeled as the sum of the spectra of pure a-Ge:H, pure a-Si:H, and a-SiGe:H alloy. The effective thickness of the a-Si:H sublayer in this sample is 0.8 nm, and the a-Ge:H sublayer thickness is 0.7 nm. We now focus on the residual in the Raman spectrum after the alloy interface layer has been subtracted. In Fig. 6(b) we show the a-Ge:H TO-mode portion of the spectrum after the alloy and a-Si:H peaks have been subtracted. We have fit the high-energy side of this peak with a Gaussian. The HWHM Δ_{Ge} is 20 ± 2 cm^{-1}, comparable to that which has been found for high-quality bulk a-Ge:H. The position of the a-Ge:H residual peak in Fig. 6(b) appears to be slightly shifted (about one wave number) to higher frequency compared to bulk a-Ge:H. The a-Si:H residual peak is shown in Fig. 6(c) and is more difficult to fit because the Si cross section is smaller. The HWHM Δ_{Si} is 30 ± 4 cm^{-1}, again comparable to high quality bulk material. The a-Si:H residual peak also appears to be shifted slightly to higher frequency relative to bulk a-Si:H. The width of the TO modes for both materials are marginally narrower than bulk materials, but the change is just within experimental error. If these changes are real they suggest that unrelaxed homogeneous strain is present in these very thin amorphous layers. At this stage we can conclude that the average bond-angle distortion in the interface layer and the two layers of pure material on either side of an interface is less than $\delta\theta=10°$. The total distortion energy is thus less than 0.25 eV/bond, and the excess energy associated with the presence of the interface is less than 0.05 eV/bond.

2. *Related observations and discussion: Si/Ge*

The absence of a signature of distortion is consistent with our expectation that the a-Si:H/a-Ge:H interface has relatively low excess distortion. We argued that the two networks are very similar both in mean atom spacing and structure. The accomodation of one network to the other could be accomplished during growth by inserting excess dangling bonds at the interface or by topological changes in the amorphous structures. An example of a topological change would be a change in the ratio of sixfold to fivefold rings.[30,31] It might also be possible to change the void density near the interface. In order to accomodate the bond-length mismatch of 5% it is necessary to distort bond angles by a comparable amount. For example, if we formed a Si/Ge interface across the (100) surface of the crystalline materials, a distortion of less than $\pm9°$ would be required in the bond angle of 109.4° in the first monolayer on either side of the interface. This distortion is comparable to distortions of $\pm10°$,[22,24] which are already present in the bulk amorphous networks. Actually this excess distortion could presumably be relaxed over a few monolayers, thereby reducing the excess distortion in any given layer to below the observable limit.

An interesting related observation is that there is no

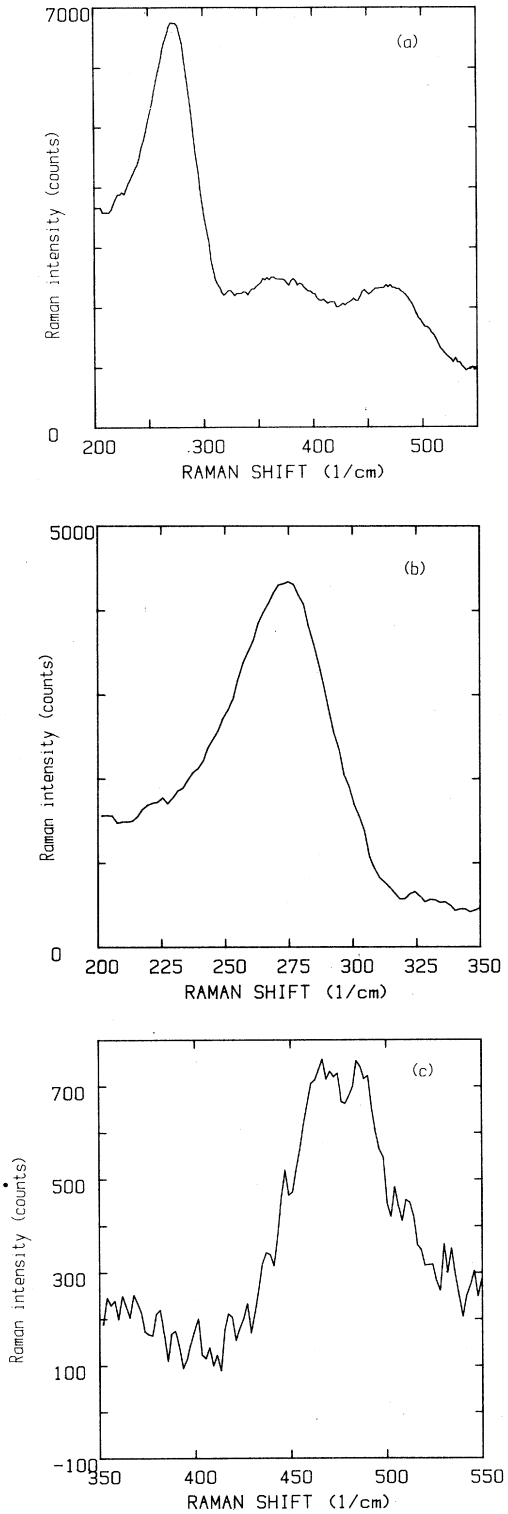

FIG. 6. (a) Raman spectrum of an *a*-Si:H/*a*-Ge:H periodic multilayer with repeat distance 2.4 nm. Excitation was with 568.2-nm light. (b) Raman spectrum from (a) after the subtraction of the spectral component due to an interfacial layer of SiGe alloy material and 0.8 nm of *a*-Si:H. The remaining signal is due to *a*-Ge:H layers with thickness of 0.7 nm. (c) Raman spectrum from (a) after subtraction of alloy interface and *a*-Ge:H components.

evidence for excess H at the *a*-Si:H/*a*-Ge:H interface.[13] One way of viewing this is that the low-distortion interface may not present an enhanced opportunity for H to substitute for strained bonds.

The density of electronic defects at the *a*-Si:H/*a*-Ge:H interface is also quite low. Space-charge limited-current measurements,[50] which yield the density of gap states near the center of the gap, imply that the density of interface states is less than 10^{10} cm^{-2}. (The measurement is limited by the density of bulk states in *a*-Ge:H.) Enhancement of photoconductivity in *a*-Ge:H layers is observed[51] as d_{Ge} is decreased. This effect is actually due to charge transfer from Ge to Si layers, but it could not be observed if the interface recombination center density exceeded the bulk density. An enhancement in the photoluminescence efficiency is also observed[52,53] for thinner *a*-Ge:H layers, this effect again requires that the density of electrically active defects near the interface not exceed the density in bulk *a*-Ge:H.

The low density of interface defects suggests that network mismatch is indeed accommodated through network distortions and not dangling bonds. If the interface mismatch were entirely accommodated by dangling bonds (misfit dislocations in crytalline heterojunctions) then the density of dangling bonds would be expected to be about 1×10^{14} cm^{-2}. Hydrogen would be expected to passivate these bonds with about the same efficiency as in the bulk materials (about 99.5%). We would then expect to observe 5×10^{11} cm^{-2} dangling bond defects at the interface. In fact the density is at least fifty times lower than this.

IV. DISCUSSION AND SUMMARY

We have analyzed vibrational Raman scattering data on two series of amorphous multilayer materials, *a*-Si:H/*a*-SiN$_x$:H and *a*-Si:H/*a*-Ge:H. It is possible to draw several conclusions with respect to the structure and optical properties of these heterojunction interfaces and ultrathin layers. Broadening of the *a*-Si:H transverse-optic mode as *a*-Si:H sublayer thickness is decreased in silicon–nitride multilayers leads to the conclusion that the presence of the nitride interface or nitrogen alloying in the first few monolayers near the interface causes excess network distortion in *a*-Si:H. This distortion is substantial, up to 0.5 eV/bond for atoms near the interface. Conversely no broadening is observed for either *a*-Ge:H or *a*-Si:H optic modes in *a*-Si:H/*a*-Ge:H multilayers. We attribute this difference to the fact that *a*-Ge and *a*-Si are intrinsically similar structures in which network mismatch is easily accommodated near the interface. Also, the introduction of Ge or Si impurities in a network of the opposite type does not result in large distortions because the bond lengths are nearly equal and the coordination is the same. Accomodation of network strain probably occurs by a number of mechanisms, including bond-angle deformation, topological changes, changes in void density, and dangling-bond generation. Only a few of these effects can be observed in changes in the Raman spectrum.

a-Si and *a*-SiN$_x$ are very different in structure and

average bond length, leading to large intrinsic distortions which exceed the ability of either network to accommodate without creating defects. In addition, N impurities have different bond length, charge, and coordination. We believe that the excess distortion at and near the silicon–nitride interface creates an opportunity for excess H to bond near the interface. This excess H would in turn reduce the average distortion, as it is known to do in bulk *a*-Ge:H (Ref. 25) and *a*-Si:H (Ref. 54), but it does not appear to do the whole job; the residual distortion is still large. Excess dangling bonds are found at the interface but their density depends sensitively on details of materials preparation, suggesting that their density depends on passivation efficiency.

Quantitative analysis of the Raman data tells us that the spatial extent of interface-induced network distortion is small, of the order of one to two monolayers. Intermixing of sublayer components is thus also limited to one monolayer.

Structural models of the *a*-Si/*a*-Ge and *a*-Si:/*a*-SiN_x interfaces have not been published. The structure of *a*-SiN_x is not known. At this time the best models for comparison to these experiments are those of the crystal–amorphous-solid interface in the form of (crystalline silicon)–(amorphous silicon) (*c*-Si/*a*-Si) and (crystalline silicon)–(amorphous silicon oxide) [*c*-Si/*a*-SiO_2]. These models consist of hand-built ball-and-stick models which are digitized and then relaxed on a computer.[55,56] In the case of the *c*-Si/*a*-Si interface, the average atom density far from the interface should be equal on the two sides, and therefore we do not necessarily expect to find dangling bonds. Indeed it is possible to build models with no interface dangling bonds. From these models it is possible to estimate the perpendicular distance from the interface over which the lattice and network distortion relax to the bulk values; this distance is of the order of two monolayers on either side. The excess energy associated with lattice and network distortion is about 200 meV per atom or 0.1 mJ cm^{-2}, of the same order of magnitude as that of the *a*-Si–(silicon nitride) interface. Models of the *c*-Si/*a*-SiO_2 interface yield the same result; that the structural difference can be accommodated by lattice and network distortions within a few monolayers on either side of the interface[57] with only a very small density of dangling bonds. Correlations between the present results and models should be treated with caution. First, the systems are quite different. Second, it has been pointed out[58] that conclusions from models of this type may be questionable because they originate with hand-built models which may incorporate a large number of human decisions which may in turn bias the results even if the model is relaxed later. It is certainly not clear that nature will choose the approach that we find easiest to model.

We also report for the first time a change in the Raman cross section for *a*-Si which is dependent upon the thickness of the *a*-Si layer. We interpret this as a resonant Raman effect due to the shift in the optical band gap of *a*-Si:H as the layer thickness is decreased. Resonant Raman scattering can thus be applied even when only a small number of laser lines are available. In order to observe quantum-size sublevels by resonant Raman scattering it is necessary to have a large number of samples with closely spaced repeat distances, or a larger number of laser lines. Resonant Raman studies with a dye laser could be used as a form of modulation spectroscopy to study resonances due to quantum effects on the optical properties.[20]

The present study demonstrates the power of vibrational Raman scattering as a probe of structure and strain in amorphous heterojunctions. Studies of this type on technologically important amorphous heterojunction systems as a function of preparation and processing may be expected to yield new and useful information.

ACKNOWLEDGMENTS

The author gratefully acknowledges many useful discussions with Ben Abeles, A. Ruppert, C. Roxlo, and T. Tiedje. The assistance of Y.-C. Wu with data reduction is also acknowledged. Samples for this work were supplied by B. Abeles of Exxon Research and Engineering Company (Annandale, NJ). Part of this work was carried out at Exxon Research and Engineering Company. Supported in part by the National Science Foundation under Grant No. DMR-87-14634 and by Rensselaer Polytechnic Institute.

[1] *Interfaces, Superlattices, and Thin Films,* edited by J. Dow and I. Schuller (Materials Research Society, Pittsburgh, 1987), and references therein.

[2] *Multilayers: Non-Electronic Properties,* edited by T. Barbee, F. Spaepen (Materials Research Society, Pittsburgh, 1988).

[3] See for example, *Material Analysis by Ion Channeling,* edited by L. C. Feldman, J. W. Mayer, and S. T. Picraux (Academic, New York, 1982).

[4] B. C. Cooman, J. R. Conner, S. R. Summerfelt, S. McKernan, C. B. Carter, and J. R. Shealy, in Ref. 1, p. 187.

[5] S. Wagner, Jpn. J. Appl. Phys., PT. 2 **24**, L155 (1985).

[6] D. E. Polk, J. Non-Cryst. Solids **5**, 365 (1971).

[7] C. Roxlo and B. Abeles, Phys. Rev. B **34**, 2522 (1986).

[8] L. Yang, B. Abeles and P. Persans, Appl. Phys. Lett. **49**, 631 (1986).

[9] L. Yang and B. Abeles, in Ref. 1 , p. 641.

[10] A. F. Ruppert, P. Persans, K. Liang, G. Hughes, B. Abeles, and H. Stasiewski (unpublished).

[11] B. Abeles, L. Yang, P. Persans, H. Stasiewski, and W. Lanford, Appl. Phys. Lett. **48**, 168 (1986).

[12] P. D. Persans, B. Abeles, A. F. Ruppert, T. Tiedje, and H. Stasiewski, J. Phys. (Paris) Colloq. **46**, C8-597 (1985).

[13] P. D. Persans, B. Abeles, J. Scanlon, and H. Stasiewski, *Proceedings of the 17th International Conference on the Physics of Semiconductors,* edited by J. Chadi and W. A. Harrison (Springer-Verlag, New York, 1985), p. 499.

[14] D. Bermejo, M. Cardona, and M. H. Brodsky, in *Proceedings of the 7th International Conference on Amorphous and Liquid Semiconductors,* edited by W. Spear (University of Edinburgh, 1977), p. 343.

[15]D. Bermejo and M. Cardona, J. Non-Cryst. Solids **32**, 405 (1979).
[16]W. Paul and D. Anderson, Solar Energy Mater. **5**, 229 (1981).
[17]H. Ugur and H. Fritzsche, Solid State Commun. **52**, 649 (1984).
[18]R. W. Collins, Phys. Rev. B **34**, 2910 (1986).
[19]B. Abeles and T. Tiedje, Phys. Rev. Lett. **51**, 2003 (1983).
[20]K. Hattori, T. Mori, H. Okamoto, and Y. Hamakawa, Phys. Rev. Lett. **60**, 825 (1988).
[21]R. Tsu, J. G. Hernandez, and F. H. Pollak, J. Non-Cryst. Solids **66**, 109 (1984).
[22]D. Beeman, R. Tsu, and M. F. Thorpe, Phys. Rev. B **32**, 874 (1985).
[23]N. Maley, L. J. Pilione, S. T. Kshirsagar, and J. S. Lannin, Physica Amsterdam **117B/118B**, 880 (1983).
[24]J. S. Lannin, Bull. Am. Phys. Soc. **33**, 474 (1988).
[25]P. D. Persans, A. F. Ruppert, S. Chan, and G. D. Cody, Solid State Commun. **51**, 203 (1984).
[26]P. D. Persans, A. F. Ruppert, G. D. Cody, and B. G. Brooks, in *Optical Effects in Amorphous Semiconductors,* edited by P. C. Taylor and S. G. Bishop (American Institute of Physics, New York, 1984), p. 349.
[27]N. Maley, J. S. Lannin, and H. Ugur, J. Non-Cryst. Solids **77/78**, 1073 (1985).
[28]N. Maley and J. S. Lannin, Phys. Rev. B **31**, 5577 (1985).
[29]P. D. Persans and A. F. Ruppert, in *Semiconductor-Based Heterostructures: Interfacial Structure and Stability,* edited by M. L. Green (Materials Research Society, Pittsburgh, 1986).
[30]D. Beeman and B. Bobbs, Phys. Rev. B **12**, 1399 (1975).
[31]P. E. Meek, Philos. Mag. **33**, 897 (1976).
[32]R. M. Martin, Phys. Rev. B **1**, 4005 (1970).
[33]C. B. Roxlo, B. Abeles, and P. D. Persans, J. Vac. Soc. Technol. B **4**, 1430 (1986).
[34]A. Morimoto, S. Oozora, M. Kumeda, and T. Shimizu, Solid State Commun. **47**, 773 (1983).
[35]P. V. Santos and L. Ley, Phys. Rev. B **36**, 3325 (1987).
[36]T. H. Engleret, G. Abstreiter, and G. Pontchara, Solid State Electron. **23**, 31 (1980).
[37]S. Minomura, in *Solid State Physics Under Pressure,* edited by S. Minomura (Kluwer Academic, Hingham, England, 1986), p. 275.
p. 275.
[38]R. Carius, K. Jahn, W. Siebert, and W. Fuhs, J. Lumin. **31/32**, 354 (1984).
[39]I. Austin, W. Jackson, T. Searle, P. Bhat, and R. Gibson, Philos. Mag. B **52**, 271 (1985).
[40]C. Roxlo, B. Abeles, and P. Persans, Appl. Phys. Lett. **45**, 1132 (1984).
[41]B. Abeles, P. D. Persans, H. Stasiewski, and W. Lanford, J. Non-Cryst. Solids **77/78**, 1065 (1985).
[42]C. Roxlo, B. Abeles, and T. Tiedje, Phys. Rev. Lett. **52**, 1994 (1984).
[43]T. Tiedje, B. Abeles, and B. Brooks, in Ref. 26, p. 417.
[44]P. G. Lecomber, W. E. Spear, R. A. Gibson, M. Hopkinson, P, K. Bhat, T. M. Searle, and I. G. Austin, J. Non-Cryst. Solids **77/78**, 1081 (1985).
[45]T. Tiedje and B. Abeles, Appl. Phys. Lett. **45**, 179 (1984).
[46]B. Wilson, Solid State Commun. **55**, 105 (1985).
[47]R. Street and M. J. Thompson, in Ref. 26, p. 410.
[48]P. Persans, A. F. Ruppert, B. Abeles, and T. Tiedje, Phys. Rev. B **32**, 5558 (1985).
[49]D. Allred, J. Gonzalez-Hernandez, O. X. Nguyen, D. Martin, and D. Pawlik, J. Mater. Res. **1**, 468 (1986).
[50]C. Wronski, P. D. Persans, and B. Abeles, Appl. Phys. Lett. **49**, 571 (1986).
[51]C. Wronski, T. Tiedje, P. Persans, B. Abeles, and M. Hicks, Appl. Phys. Lett. **49**, 1378 (1986).
[52]T. Tiedje, C. Wronski, P. Persans, and B. Abeles, J. Non-Cryst. Solids **77/78**, 1031 (1985).
[53]T. Tiedje, B. Abeles, and B. Brooks, Phys. Rev. Lett. **54**, 2545 (1985).
[54]G. D. Cody, T. Tiedje, B. Abeles, B. Brooks, and Y. Goldstein, Phys. Rev. Lett. **47**, 1480 (1981).
[55]F. Spaepen, Acta Met. **26**, 1167 (1978).
[56]T. Saito and I. Ohdomari, Philos. Mag., **B43**, 673 (1981).
[57]S. T. Pantelides and M. Long, in *The Physics of SiO_2 and Its Interfaces,* edited by S. T. Pantelides (Pergamon, New York, 1978), p. 339.
[58]F. Herman and P. Lambin, in *Tetrahedrally-Bonded Amorphous Semiconductors,* edited by D. Adler and H. Fritzsche (Plenum, New York, 1985), p. 469.